Comparison of Symmetrical and Unsymmetrical Structures in the Performance of Reflective Multiband Metasurfaces

Taufiqqurrachman, *Member, IAENG*, Mohamad Kamal B. A. Rahim, Noor Asmawati Binti Samsuri, Yusuf Nur Wijayanto, Nur Syahirah Mohd Yaziz, and Sunusi Garba Mohammed

***Abstract*— The metal structure on a reflective metasurface significantly impacts its performance as a reflector, particularly in supporting future wireless networks in the smart radio environment (SRE). This paper presents two configuration designs aimed at achieving a multiband response and compares their performance in terms of reflection value, reflection phase, and radar cross section (RCS) when the metal structure is rotated to 0° and 90°. The first design utilizes a multi-ring resonator, which is a symmetrical structure, while the second design employs multi split-ring resonators (SRRs), forming an asymmetrical structure. The results indicate that the symmetrical structure demonstrates slightly better performance than the asymmetrical structure, especially when rotated to 90°. Both structures achieve reflection values above 0.75 and RCS values of at least 19.2 dB(m²) at all desired frequencies when positioned at 0°.**

***Index Terms*— multiband reflective metasurface, ring resonator, split ring resonators (SRRs), symmetrical structure, unsymmetrical structure**

I. Introduction

FUTURE wireless networks envision a smart radio environment (SRE) that enhances communication links by enabling devices to intelligently adapt to their environments, thereby improving efficiency, connectivity, and overall performance. This advancement can be realized through the use of intelligent reflecting surfaces (IRSs), also known as reconfigurable intelligent surfaces (RISs), which redirect incoming electromagnetic waves from the transmitter to the receiver—effectively mitigating obstacles along the transmission path. Moreover, RISs offer several advantages, including ease of deployment, improved spectral efficiency, environmental sustainability, and system compatibility, as demonstrated in [1]–[2].

Reconfigurable intelligent surfaces (RISs) are typically implemented in three configurations: reflective, transmissive, and hybrid, as described in [3]–[4]. In the reflective configuration, each unit element reflects the incident signal, enabled by the presence of a copper backplane. In contrast, in the transmissive configuration, the copper backplane is omitted, allowing electromagnetic waves to pass through the elements. The hybrid configuration combines both functionalities, splitting the signal power between reflection and transmission. Similar to the transmissive type, hybrid RISs do not employ a copper backplane in their structure.

The core component of RISs [5] is the reconfigurable metasurface (RMS), which consists of a thin electromagnetic sheet composed of elementary elements—referred to as unit cells or meta-atoms—that can be dynamically configured. The RMS exhibits three key features: configurability, near-passive implementation, and multifunctional wave shaping. This multifunctionality enables the metasurface to simultaneously perform various operations, such as reflection, refraction, and blocking of incident radio waves. For reflective applications, the RMS is typically composed of multiple reflective metasurface unit cells, in which both the incident and reflected signals reside on the same side of the surface, as reported in [6].

The physically based modeling of RISs accounts for several key characteristics, including reconfigurability, oblique incidence effects (spatial dispersion), mutual coupling between closely spaced unit cells, and reflection losses, as reviewed in [7]. The impacts of reflection losses and oblique incidence are further explored at the unit cell level in [8] and [9]. Specifically, [8] presents a comparative analysis of reflection losses between circular and hexagonal geometries, while [9] investigates the oblique incidence behavior of circular-shaped unit cells.

Several structures have been designed and demonstrated to manipulate electromagnetic waves using PIN or varactor diodes, as reported in [10]–[14]. A binary tunable design in [10] features a rectangular patch serving as a reflector and a parasitic strip with a single PIN diode, enabling tunable

Manuscript received November 4, 2024; revised July 30, 2025.

This work was supported by the Ministry of Higher Education (MOHE) under grant no. FRGS/1/2021/STG04/UTM/01/1, Research Management Center (RMC) at the Faculty of Electrical Engineering, Universiti Teknologi Malaysia (UTM), under grant no. 04M37, and the National Research and Innovation Agency (BRIN) through funding for the Rumah Program Prototype of IoT Telecommunications System Innovation Research for fiscal year 2025.

Taufiqqurrachman is a PhD student at the Advanced RF and Microwave Research Group (ARFMRG) in Universiti Teknologi Malaysia (UTM), Johor Bahru, Malaysia (e-mail: taufiqqurrachman@gmail.com).

Mohamad Kamal B. A. Rahim is a professor at the Advanced RF and Microwave Research Group (ARFMRG) in Universiti Teknologi Malaysia (UTM), Johor Bahru, Malaysia (e-mail: mdkamal@utm.my).

Noor Asmawati Binti Samsuri is a senior lecturer at the Advanced RF and Microwave Research Group (ARFMRG) in Universiti Teknologi Malaysia (UTM), Johor Bahru, Malaysia (e-mail: asmawati@utm.my).

Yusuf Nur Wijayanto is a research professor at the National Research and Innovation Agency (BRIN), Bandung, 40135, Indonesia (e-mail: ynwijayanto@gmail.com).

Nur Syahirah Mohd Yaziz is a PhD student at the Advanced RF and Microwave Research Group (ARFMRG) in Universiti Teknologi Malaysia (UTM), Johor Bahru, Malaysia (e-mail: syahirahyaziz@gmail.com).

Sunusi Garba Mohammed is a PhD student at the Advanced RF and Microwave Research Group (ARFMRG) in Universiti Teknologi Malaysia (UTM), Johor Bahru, Malaysia (e-mail: sgmohammed.ele@buk.edu.ng).

resonance between two states: 0 and π. Similarly, [11] presents a microwave structure incorporating a PIN diode to achieve binary switching between the same two states. In [12], a varactor diode is integrated into a rectangular patch with two gaps, each hosting a varactor diode to control both the amplitude and phase of the reflected signal. The design in [13] introduces a reconfigurable intelligent surface (RIS) composed of two D-shaped patches connected by a varactor diode. Furthermore, [14] demonstrates a dual-band RIS using a PIN diode operating at 5.8 GHz and 7.3 GHz, with each unit cell incorporating an integrated RF choke to minimize losses. However, none of these referenced works report on the effects or performance of rotating structures.

This paper presents a performance comparison between symmetrical and unsymmetrical structures in terms of the multiband response of both unit cells and macrocells. The symmetrical structure is represented by the multi-ring resonator, while the unsymmetrical structure is realized using split-ring resonators (SRRs). A key objective is to evaluate whether the rotation of these structures impacts the performance of multiband reflective metasurfaces in real environments.

II. Design Concept

The proposed design consists of two configurations implemented on the top layer, as illustrated in Fig. 1. The first configuration features a symmetrical structure composed of multiple ring resonators (Fig. 1a and 1c), while the second employs an unsymmetrical structure comprising multiple split-ring resonators (SRRs) (Fig. 1b and 1d). Both configurations are designed on F4BMX220 substrate with a thickness of 1.5 mm, a dielectric constant of 2.2, and a loss tangent of 0.001. A full ground plane is incorporated on the bottom layer of the substrate to ensure effective signal reflection. The targeted resonance frequencies for both structures are 8, 10, and 12 GHz.

The first proposed design, which incorporates multi-ring resonators, employs the following equations to determine the physical dimensions of each ring [15], [16]:

For $^{wr}/_{h} \leq 1$,

$$\varepsilon_{re} = \frac{\varepsilon_r+1}{2} + \frac{\varepsilon_r+1}{2}\left(\left(1+12\frac{h}{wr}\right)^{-0.5} + 0.04\left(1-\frac{wr}{h}\right)^{2}\right) \quad (1)$$

$$R = \frac{R_i+R_0}{2} \quad (2)$$

$$f_o(GHz) = \frac{300}{\pi(R_i+R_0)\sqrt{\varepsilon_{re}}} \quad (3)$$

where f_o is the resonance frequency, ε_{re} is the effective dielectric constant, wr is the width of the ring, h is the substrate height, and R is the ring radius.

The second proposed design, which consists of multiple split-ring resonators (SRRs), uses the following equations to determine the physical dimensions of each ring [17]:

$$f_r = \frac{1}{2\pi\sqrt{LC_T}} \quad (4)$$

$$L = \mu_0 R_m\left(\ln\left(\frac{8R_m}{h+wr}\right) - 0.5\right) \quad (5)$$

$$R_m = R + \frac{wr}{2} \quad (5.a)$$

$$C_T = C_{gap} + C_{surface} \quad (6)$$

$$C_{gap} = \varepsilon_0\left|\frac{wr\ h}{gap} + \frac{2\pi\ h}{\ln\left(\frac{2.4\ h}{wr}\right)}\right| \quad (6.a)$$

$$C_{surface} = \frac{2\ h\ \varepsilon_0\ \varepsilon_r}{\pi}\ln\left(\frac{4\ R}{gap}\right) \quad (6.b)$$

where f_r is the resonance frequency, R is the radius of the SRR, L is the inductance of the resonator, C_T is total capacitance resulting from the parallel combination of the gap capacitance (C_{gap}) and the capacitance surface ($C_{surface}$), and gap is the gap width in the resonator.

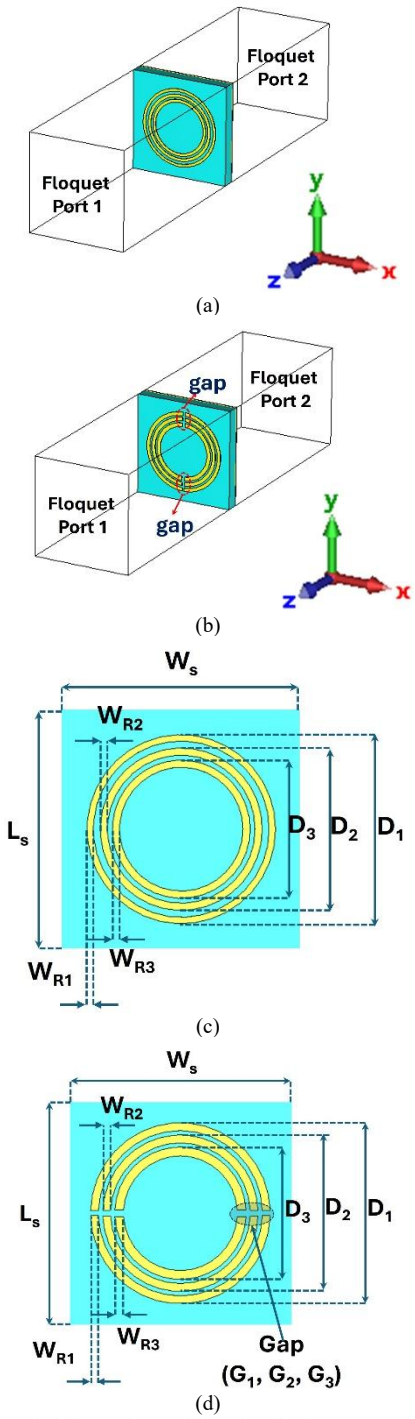

Fig. 1. Proposed design of a multiband reflective metasurface at the 0° structural position: (a) symmetrical structure, (b) unsymmetrical structure, (c) dimensions of the symmetrical structure, and (d) dimensions of the unsymmetrical structure.

The optimized dimensions of both structures, as presented in Table I, were obtained through CST optimization to

achieve the optimal performance. The unsymmetrical structure, consisting of multiple SRRs, features a larger ring radius and width compared to the symmetrical structure. However, both structures occupy the same substrate area of 11.43 x 11.43 mm² for one unit cell.

TABLE I
OPTIMIZED DIMENSIONS OF THE SYMMETRICAL AND UNSYMMETRICAL STRUCTURES

Parameters	Values in mm	
	Symmetrical (Multi Rings)	Unsymmetrical (Multi SRRs)
W_s, L_s	11.43	
D_1	8.96	9.2
D_2	7.7	7.95
D_3	6.55	6,75
Wr_1	0.3	0.4
Wr_2	0.34	0.4
Wr_3	0.34	0.45
G_1	-	0.25
G_2	-	0.3
G_3	-	0.35

Fig. 2 illustrates the equivalent circuit model of the reflective metasurface, which includes the free-space impedance (Z_0), the surface impedance (Z_s), and the dielectric slab. The surface impedance (Z_s) represents the impedance of the metasurface structure and can be calculated using the following equation, as presented in [13]:

$$Z_{in} = j\frac{Z_0}{\sqrt{\varepsilon_r}}\tan(k_0\sqrt{\varepsilon_r}h) \quad (7)$$

$$Z_s = Z_0 Z_{in}\frac{1+S_{11}}{Z_{in}(1-S_{11})-Z_0(1+S_{11})} \quad (8)$$

where $k_0 = {}^{2\pi}/_{\lambda}$

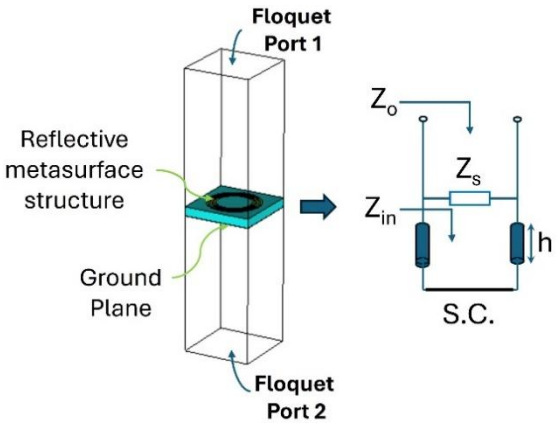

Fig. 2. The equivalent circuit model of the reflective metasurface.

III. RESULTS AND DISCUSSION

The multi-SRRs with an unsymmetrical structure are designed to rotate, as illustrate in Fig. 3. In the 0° position, the gapis oriented horizontally, while in the 90° position, the gap is oriented vertically. In contrast, the multi-ring resonators, with a symmetrical structure, remain unaffected by rotation and perform identically in both the 0° and 90° positions.

The results present the S-parameters, reflection phase, and radiation pattern graphs for both proposed designs, as shown in Fig. 4 to 5. These results illustrate the comparative performance of the designs as their structures are rotated at 0° and 90°.

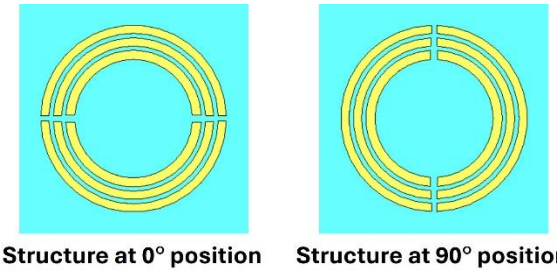

Fig. 3. Unsymmetrical structure at 0°and 90°.

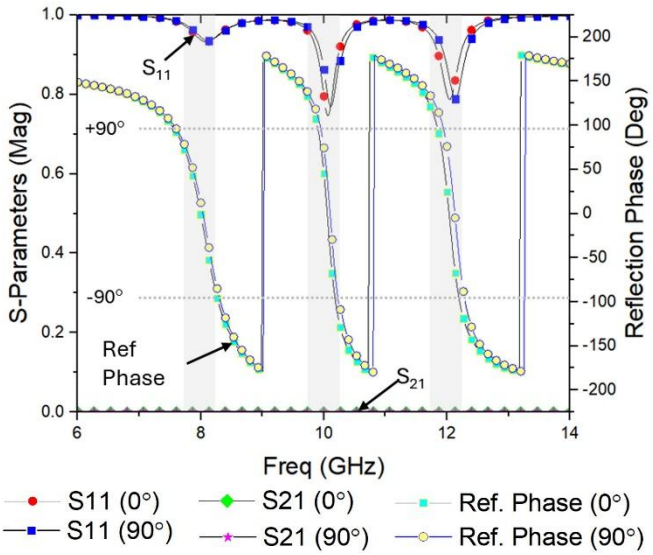

Fig. 4. S-Parameters and reflection phase of the symmetrical structure for rotating structures at 0° and 90°.

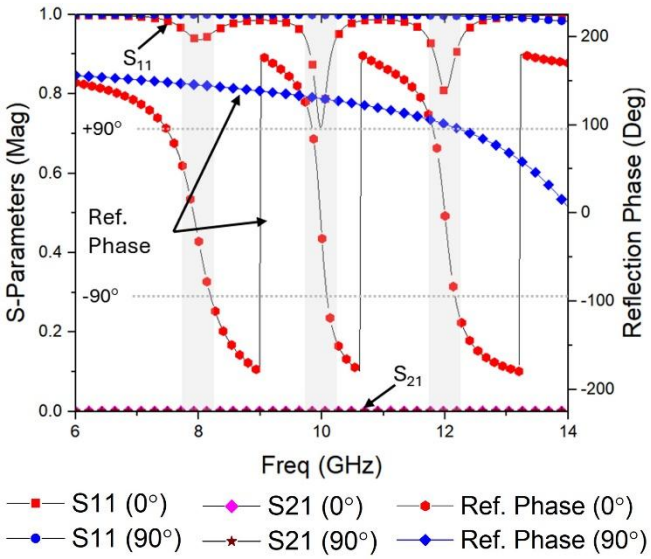

Fig. 5. S-Parameters and reflection phase of the unsymmetrical structure for rotating structures at 0° and 90°.

In the symmetrical structure, as shown in Fig. 4, the S_{11} parameter exhibits three resonance frequencies for the rotating structures at 0° and 90°, with slight shifts in both frequency and amplitude. The reflection phase for these angles shows a minor shift towards lower frequencies. However, the S_{21} value at all resonance frequencies

indicates that the signal cannot pass through the proposed design and is reflected back, resulting in an S_{21} value of zero.

The unsymmetrical structure, shown in Fig. 5, demonstrates that the S_{11} parameter exhibits three resonance frequencies at 0° position, but no resonance frequency is observed at 90° position. Similarly, the reflection phase graph shows resonance frequencies at 8, 10, and 12 GHz at 0° position, while these frequencies do not appear at 90° position. The S_{21} parameter remains at zero, indicating that incoming signals are reflected back.

Using the equation (7) and (8), the surface impedance (Z_s) for both structures at the 0° rotation is calculated as follows: $-j0.946\ \Omega$ at 8 GHz, $-j1.179\ \Omega$ at 10 GHz, and $-j1.419\ \Omega$ at 12 GHz. For the symmetrical structure at the 90° rotation, the Z_s value has $-j0.947\ \Omega$ at 8 GHz, $-j1.184\ \Omega$ at 10 GHz, and $-j1.418\ \Omega$ at 12 GHz, showing no significant change due to the symmetry of the structure. However, for the unsymmetrical structure at a 90° rotation, the Z_s value cannot be calculated due to the lack of resonance at all frequencies.

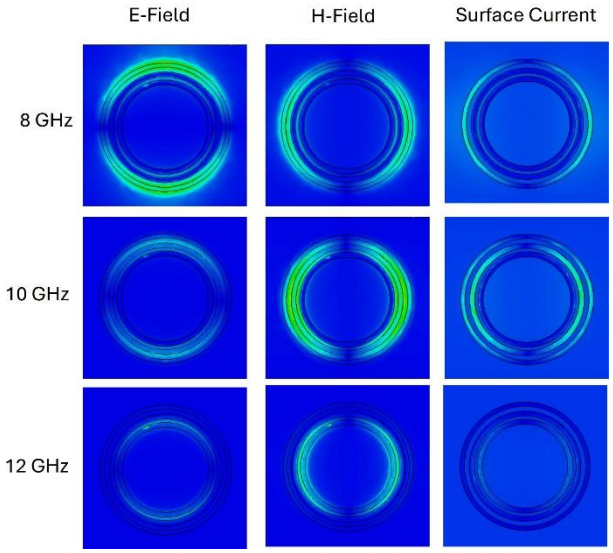

Fig. 6. Electromagnetic wave properties of the multiple-ring resonator structure (symmetrical structure).

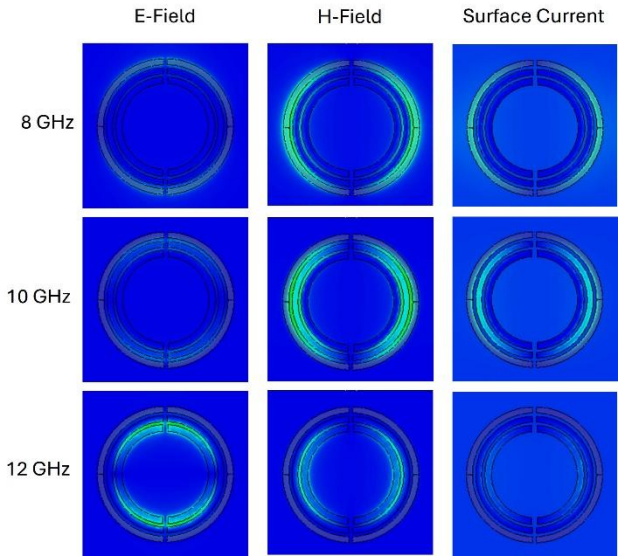

Fig. 7. Electromagnetic wave properties of the multiple-split ring resonator structure (unsymmetrical structure).

Fig. 6 and 7 present the electromagnetic wave properties of both symmetrical and unsymmetrical structures, indicated by the intensities of the E-field, H-field, and surface current. In the symmetrical structure, shown in Fig. 6a, the E-field intensity is highest at the resonance frequency of 8 GHz, though it is distributed both above and below each ring depending on the resonance frequency. Meanwhile, the H-field and surface current intensities, shown in Fig. 6b and 6c, are strongest at the resonance frequency of 10 GHz due to the coupling among the rings. Additionally, the H-field intensity is observed on both the right and left sides of each ring at this resonance frequency.

On the other hand, the E-field intensity is highest at 12 GHz, as shown in Fig. 7a, with the intensity distributed both above and below each ring. The H-field intensity, shown in Fig. 7b, is highest at 10 GHz, with distribution on both the right and left sides of the ring due to the stronger coupling of the middle ring compared to the others. This behavior is similar to the surface current intensity, shown in Fig. 7c, where the surface current intensity is also highest at 10 GHz. Based on Fig. 7, the gap in the unsymmetrical structure contributes to the higher intensity of the E-field.

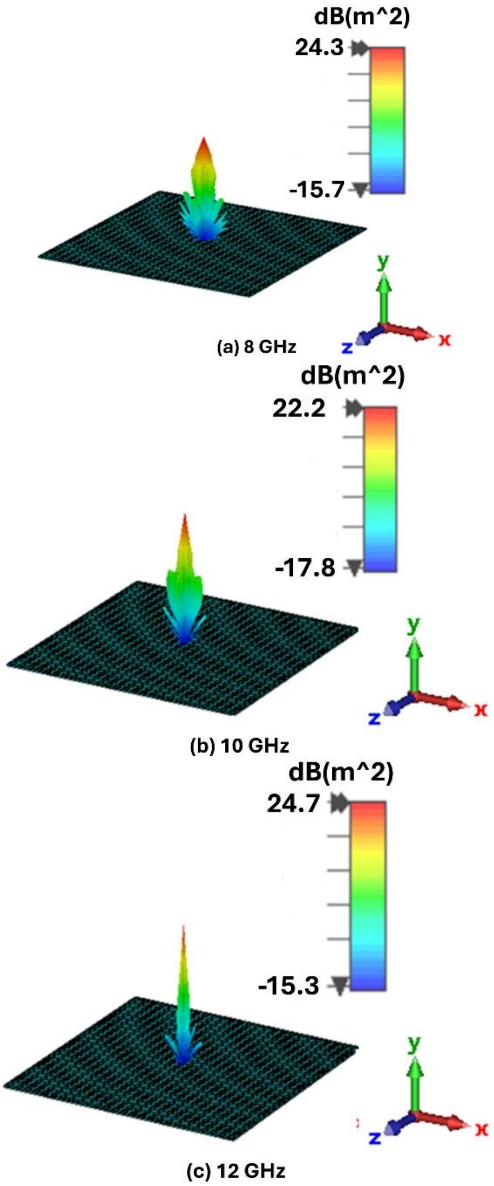

Fig. 8. Radiation pattern for the symmetrical structure at each desired frequency when the structure is rotated to 0° and 90°.

The full structure of the multiband reflective metasurface consists of 26 x 26-unit cells, covering an area of 297.18 x 297.18 mm². The radiation pattern in Fig. 8 shows similar results for the symmetrical structure at both 0° and 90°, with RCS values of 24.3 dB(m²) at 8 GHz, 22.2 dB(m²) at 10 GHz, and 24.7 dB(m²) at 12 GHz. In contrast, the radiation pattern of the unsymmetrical structure depicted in Fig. 9 and 10 indicate that the RCS values for the 0° and 90° structural positions differ.

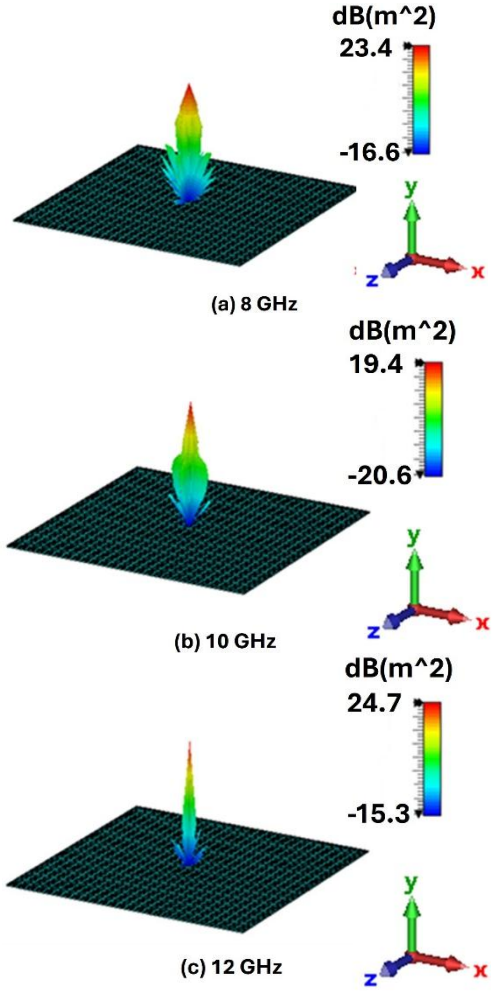

Fig. 9. Radiation pattern for the unsymmetrical structure at each desired frequency when the structure is rotated to 0°.

At the normal position of the multi SRRs (0°), the RCS value reaches 23.4 dB(m²) at 8 GHz, 19.4 dB(m²) at 10 GHz, and 24.7 dB(m²) at 12 GHz, as shown in Fig. 9. In contrast, when the structure is rotated to 90° as shown in Fig. 10, the RCS values are -28.8 dB(m²) at 8 GHz, 7.68 dB(m²) at 10 GHz, and 18.2 dB(m²) at 12 GHz. This indicates that the structure does not achieve optimal performance when positioned away from 0°, due to the differences in structure orientation between 0° and 90°. In other words, the symmetrical structure with multi-ring resonators can be placed at any rotation angle in the real environments without reducing the performance of the multiband reflective metasurface. However, the asymmetrical structure with multi SRRs should be positioned at the 0° orientation in the real environments to achieve optimal performance.

Based on Table II, the multi SRRs at the 0° position show a slightly better response in the S_{11} (reflection) value compared to the multi rings, particularly at the higher frequencies of 10 and 12 GHz. Both structures, multi rings and SRRs, exhibit a zero value for S_{21} at all desired frequencies, indicating that the incoming signal is reflected back due to the full ground plane at the back of both structures. The RCS value for both structures exceeds 20 dB(m²), except at 10 GHz for the multi SRRs structure.

The multi rings structure at the 90° position shows results similar to those at the 0° position. However, the multi SRRs structure at the 90° position does not perform well in terms of the S_{11} value due to structural changes. The RCS value at the 90° position for the multi SRRs is negative only at 8 GHz and positive at 10 and 12 GHz, but overall performance is not satisfactory.

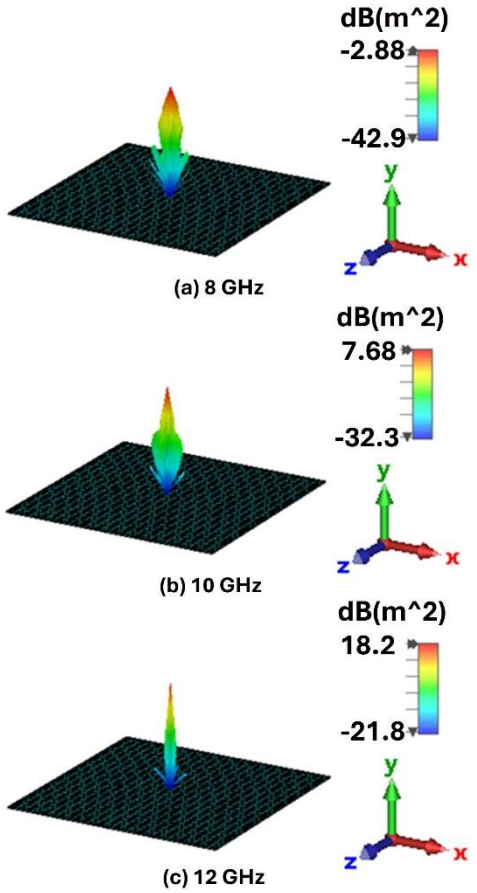

Fig. 10. Radiation pattern for the unsymmetrical structure at each desired frequency when the structure is rotated to 90°.

TABLE II
COMPARISON OF S-PARAMETERS, REFLECTION PHASE AND RCS BETWEEN SYMMETRICAL AND UNSYMMETRICAL STRUCTURES

Parameters		Value if the structure is rotate to :			
		0°		90°	
		Multi Rings	Multi SRRs	Multi Rings	Multi SRRs
S_{11} (Mag)	8 GHz	0.94	0.94	0.94	0.999
	10 GHz	0.79	0.72	0.84	0.999
	12 GHz	0.8	0.8	0.81	0.997
S_{21} (Mag)	8 GHz	0			
	10 GHz				
	12 GHz				
Reflection Phase (Deg)	8 GHz	-0.92	-32.2	2.52	145.1
	10 GHz	45.4	-29.1	59.2	129.7
	12 GHz	24.8	-3.3	33	100.7
RCS (dB(m²))	8 GHz	24.26	23.4	24.26	-28.8
	10 GHz	22.2	19.4	22.2	7.68
	12 GHz	24.7	24.7	24.7	18.2

Table III presents the bandwidth comparison between the symmetrical and unsymmetrical structures at the 0° and 90° positions. For the symmetrical structure, represented by multiple rings, the bandwidth values at 8 GHz and 10 GHz are nearly identical for both orientations, 0.613 GHz and 0.24 GHz, respectively. At 12 GHz, the bandwidth differs slightly between the 0° and 90° positions: 0.267 GHz and 0.29 GHz, respectively. For the unsymmetrical structure, represented by multiple SRRs, the bandwidth is considered only at the 0° position, yielding 0.613 GHz at 8 GHz, 0.19 GHz at 10 GHz, and 0.29 GHz at 12 GHz. At 90° position, the bandwidth cannot be calculated due to no resonance frequencies.

TABLE III
BANDWIDTH COMPARISON BETWEEN SYMMETRICAL AND UNSYMMETRICAL STRUCTURES

Parameters		Value if the structure is rotate to :			
		0°		90°	
		Multi Rings	Multi SRRs	Multi Rings	Multi SRRs
Bandwidth (GHz)	8 GHz	0.613	0.613	0.613	-
	10 GHz	0.24	0.19	0.24	-
	12 GHz	0.267	0.29	0.29	-

When comparing the bandwidths of the symmetrical and unsymmetrical structures at 10 GHz, the symmetrical structure exhibits a slightly wider bandwidth, with a difference of approximately 0.05 GHz. This difference is attributed to stronger coupling effects in the unsymmetrical structure, caused by the presence of gaps within and between the rings.

IV. CONCLUSION

The symmetrical and unsymmetrical structures were designed to operate at multiple frequencies: 8, 10, and 12 GHz. The symmetrical structure employs multi-ring resonators, while the unsymmetrical structure uses multi-split ring resonators (SRRs). Based on the results, both structures demonstrate good performance in terms of S_{11} and radar cross-section (RCS) values at the normal (0°) position, with S_{11} values above 0.79 and RCS values exceeding 20 dB(m²) across all target frequencies. However, the performance of the multi-SRRs degrades significantly when the structure is rotated to 90°. Overall, the multi-ring resonators exhibit superior performance compared to the multi-SRRs, as their functionality remains consistent regardless of the orientation.

REFERENCES

[1] Y. Liu et al., "Reconfigurable Intelligent Surfaces: Principles and Opportunities," in IEEE Communications Surveys & Tutorials, vol. 23, no. 3, pp. 1546-1577, third quarter 2021, doi: 10.1109/COMST.2021.3077737.

[2] E. Basar, M. Di Renzo, J. De Rosny, M. Debbah, M. -S. Alouini and R. Zhang, "Wireless Communications Through Reconfigurable Intelligent Surfaces," in IEEE Access, vol. 7, pp. 116753-116773, 2019, doi: 10.1109/ACCESS.2019.2935192.

[3] S. Zeng et al., "Reconfigurable Intelligent Surfaces in 6G: Reflective, Transmissive, or Both?," in IEEE Communications Letters, vol. 25, no. 6, pp. 2063-2067, June 2021, doi: 10.1109/LCOMM.2021.3062615.

[4] Hongliang Zhang, Boya Di, Lingyang Song, Zhu Han, Reconfigurable Intelligent Surface-Empowered 6G, Springer, Switzerland, ISBN: 978-3-030-73498-5, 2021.

[5] H. Gacanin and M. Di Renzo, "Wireless 2.0: Toward an Intelligent Radio Environment Empowered by Reconfigurable Meta-Surfaces and Artificial Intelligence," in IEEE Vehicular Technology Magazine, vol. 15, no. 4, pp. 74-82, Dec. 2020, doi: 10.1109/MVT.2020.3017927.

[6] M. Di Renzo et al., "Smart Radio Environments Empowered by Reconfigurable Intelligent Surfaces: How It Works, State of Research, and The Road Ahead," in IEEE Journal on Selected Areas in Communications, vol. 38, no. 11, pp. 2450-2525, Nov. 2020, doi: 10.1109/JSAC.2020.3007211.

[7] F. Costa and M. Borgese, "Electromagnetic Model of Reflective Intelligent Surfaces," in IEEE Open Journal of the Communications Society, vol. 2, pp. 1577-1589, 2021, doi: 10.1109/OJCOMS.2021.3092217.

[8] T. Taufiqqurrachman, Y. N. Wijayanto, M. K. B. A. Rahim and N. A. Binti Samsuri, "Comparison Study of Ring Resonator Shape for Multiband IRS Application," 2023 IEEE International Symposium on Antennas and Propagation (ISAP), Kuala Lumpur, Malaysia, 2023, pp. 1-2, doi: 10.1109/ISAP57493.2023.10388647.

[9] Taufiqqurrachman, M. K. B. A. Rahim, N. A. B. Samsuri and Y. N. Wijayanto, "Multiband X-Band Frequency for Reflecting Intelligent Surfaces (IRSs)," 2023 IEEE International Symposium on Antennas and Propagation and USNC-URSI Radio Science Meeting (USNC-URSI), Portland, OR, USA, 2023, pp. 1343-1344, doi: 10.1109/USNC-URSI52151.2023.10238061.

[10] Nadège Kaina, Matthieu Dupré, Mathias Fink, and Geoffroy Lerosey, "Hybridized resonances to design tunable binary phase metasurface unit cells," Opt. Express 22, 18881-18888 (2014).

[11] M. Ouyang, F. Gao, Y. Wang, S. Zhang, P. Li and J. Ren, "Computer Vision-Aided Reconfigurable Intelligent Surface-Based Beam Tracking: Prototyping and Experimental Results," in IEEE Transactions on Wireless Communications, vol. 22, no. 12, pp. 8681-8693, Dec. 2023, doi: 10.1109/TWC.2023.3264752.

[12] X. Pei et al., "RIS-Aided Wireless Communications: Prototyping, Adaptive Beamforming, and Indoor/Outdoor Field Trials," in IEEE Transactions on Communications, vol. 69, no. 12, pp. 8627-8640, Dec. 2021, doi: 10.1109/TCOMM.2021.3116151.

[13] A. Araghi et al., "Reconfigurable Intelligent Surface (RIS) in the Sub-6 GHz Band: Design, Implementation, and Real-World Demonstration," in IEEE Access, vol. 10, pp. 2646-2655, 2022, doi: 10.1109/ACCESS.2022.3140278.

[14] Safpbri Johari, Mohd Najib Mohd Yasin, Arif Mawardi Ismail, Liya Yusrina Sabila, Dwi Sulisworo, and Muhammad Miftahul Amri, "A Low-loss Miniaturized Dual-band Reconfigurable Intelligent Surface Unit Cell with An Integrated RF Choke," Engineering Letters, vol. 32, no. 8, pp1569-1576, 2024.

[15] J. S. Hong and M. J. Lancaster, "Microstrip filters for RF/Microwave applications," John Wiley & Sons, Inc., New York, 2011.

[16] A. C. Kundu and I. Awai, "Control of attenuation pole frequency of a dual mode microstrip ring resonator bandpass filter," in IEEE Transactions on Microwave Theory and Techniques, vol. 49, no. 6, pp. 1113-1117, June 2001, doi: 10.1109/22.925499.

[17] Nadin Alrayes, Mousa I. Hussein, "Metamaterial-based sensor design using split ring resonator and Hilbert fractal for biomedical application," in Sensing and Bio-Sensing Research Open Access Journal, Volume 31, 2021, 100395, ISSN 2214-1804, doi: 10.1016/j.sbsr.2020.100395.

Taufiqqurrachman received his B.Sc. in Electrical Engineering from the University of Indonesia in 2007 and his M.Sc. in Electrical Engineering from the National Taiwan University of Science and Technology in 2018. He began his research career at the Indonesian Institute of Sciences (LIPI) in 2009 and was appointed Junior Researcher in 2016. Following the integration of LIPI into the National Research and Innovation Agency (BRIN) in 2019, he continued his research activities. He is currently pursuing a Ph.D. with the ARFM Research Group at Universiti Teknologi Malaysia. His research interests include metamaterials and metasurfaces for microwave device applications. He is a member of IEEE and IAENG. He can be contacted via email at taufiqqurrachman@gmail.com.

Mohamad Kamal A. Rahim (Senior Member, IEEE) is a Professor of RF and Antenna at the Faculty of Electrical Engineering, Universiti Teknologi Malaysia. He received his B.Eng. in Electrical and Electronic Engineering from the University of Strathclyde, U.K., in 1987, M.Eng. in Science from the University of New South Wales, Australia, in 1992, and Ph.D. in Electrical Engineering from the University of Birmingham, U.K., in 2003. He began his academic career at Universiti Teknologi Malaysia in 1989 and has since held various academic positions, including Senior Lecturer and Associate Professor. His research interests include multifunction antennas, metamaterials, and millimeter-wave antenna design.